SUPPLEMENTAL DATA

ADDITIONAL EXPERIMENTAL PROCEDURES

Immunohistochemistry—Mice (C57BL/6, 18 days old) were perfused transcardially with 4 % paraformaldehyde and 0.05 % glutaraldehyde in 0.1 M sodium phosphate buffer, pH 7.4, containing 2 % polyvinylpyrrolidone (MW 25.000) for 20 min followed by an additional perfusion fixation without glutaraldehyde for 15 min. The testes were removed and postfixed in the second fixative for 30 min at 4 °C. Microslicer sections of 600 µm thickness were cryoprotected in a graded series of 10 %, 20 %, 30 % and 2.3 M sucrose solutions containing 10 % polyvinylpyrrolidone and frozen in liquid nitrogen. For visualization of the established blood-testis barrier at P18 0.6 µm ultracryo-semithin sections were prepared (Leica Ultracut UCT equipped with a Leica EMFCS) and immunolabeled with a mixture of primary antibodies for 4 h at 20 °C: mouse anti-ZO-1/FITC (Invitrogen-Zymed, 1:100) and rabbit anti-OSB/claudin 11 (Invitrogen-Zymed, 1:100). The sections were incubated with the secondary antibody: Cy3-conjugated goat anti-rabbit IgG (Invitrogen-Zymed, 1:200) for 1 h at 20 °C. After staining of the nuclei by DAPI (20 ng/ml), the sections were analyzed by fluorescence microscopy (Zeiss Axiovert 200M).

Mass spectrometric analysis of total fatty acid—Fatty acids were hydrolized from lipids, extracted and analysed by electrospray ionization (tandem) mass spectrometry [ESI-MS(/MS)] according to Valianpour et al. with minor modifications (1). In brief, testes of juvenile C57BL/6 mice were collected and pooled as follows:

Mice: C57BL/6				
Pools [#]	Testes / pool [#]	from mice / pool [#]	Age of mice [days after birth]	Total wet weight [mg]
3	8	4	6	17, 21, and 21
3	6, 6, and 8	3, 3, and 4	10	19, 21, and 24
3	4	2	15	37, 39, and 39
3	4	2	20	61, 62, and 81
3	2	1	25	53, 63, and 72

The tissue was homogenized with distilled water on ice and of each pool an aliqout of 17 mg wet weight was lyophylized in a 16 x 125mm glas vial. Dried aliquots were taken up in 3,5 ml acetonitril/37 % hydrochloric acid (4:1 v/v), sealed with a screw cab containing a teflon gasket, suspended with the help of an ultra sound bath, and hydrolized at 90 °C for 2 hours. After cooling down to room temperature, free fatty acids were extracted with 7 ml of hexane: samples were vortex-mixed for 20 s, centrifuged at 3000 rpm for 5 min, 6.5 ml of the upper phase (containing free fatty acids and hexane) was transferred to a new glass tube, and the solvent was evaporated at room temperature under a constant stream of nitrogen. Fatty acids were dissolved in 425 µl methanol of which 10 µl were inserted into a gold sputtered glas needle for nanoESI-MS(/MS). Non-hydroxylated fatty acids were detected with a MS1 scan using a cone voltage of 55 V and 2-hydroxy fatty acids with neutral loss of 46 amu scan using a cone voltage of 55 V and a collision energy of 30 eV, all in negative ion mode.

Analysis of phospholipids and cholesteryl esters—Testes of juvenile mice were collected and pooled as follows:

Mice: C57BL/6				
Pools [#]	Testes / pool [#]	from mice / pool [#]	Age of mice [days after birth]	Total wet weight [mg]
3	16	8	6	43, 39, and 37
3	2	1	25	76, 76, and 73

Tissue was homogenized with distilled water on ice, lyophilized and extracted twice with C/M/W (10/10/1) and with C/M/W (30/60/8). The combined C/M/W extracts were desalted with RP-18 column

chromatography. Lipid extracts were resolved in 100 µl of 5 mM methanolic ammonium acetate / 2 mg tissue wet weight for nanoESI-MS/MS analysis. Phosphoglycerolipids and cholesteryl esters were analyzed in nanoESI-MS/MS positve mode. Phosphatidylcholine (*precursor ion scan m/z +184, cone voltage 40 V, collision energy 35 eV*), phosphatidylethanolamine (*neutral loss scan m +141, cone voltage 40 V, collision energy 25 eV*), and phosphatidylserine (*neutral loss scan m +185, cone voltage 40 V, collision energy 22eV*) were detected according to Brügger et al. (2) and cholesteryl esters (*precursor ion scan m/z +369, cone voltage 50 V, collision energy 13 eV*) according to Liebisch et al. (3).

SUPPLEMENTAL REFERENCES

1. Valianpour, F., Selhorst, J. J., van Lint, L. E., van Gennip, A. H., Wanders, R. J., and Kemp, S. (2003) *Mol Genet Metab* **79**, 189-196
2. Brugger, B., Erben, G., Sandhoff, R., Wieland, F. T., and Lehmann, W. D. (1997) *Proc Natl Acad Sci U S A* **94**, 2339-2344
3. Liebisch, G., Binder, M., Schifferer, R., Langmann, T., Schulz, B., and Schmitz, G. (2006) *Biochim Biophys Acta* **1761**, 121-128
4. Bellve, A. R., Cavicchia, J. C., Millette, C. F., O'Brien, D. A., Bhatnagar, Y. M., and Dym, M. (1977) *J Cell Biol* **74**, 68-85
5. Wang, Y., Botolin, D., Xu, J., Christian, B., Mitchell, E., Jayaprakasam, B., Nair, M. G., Peters, J. M., Busik, J. V., Olson, L. K., and Jump, D. B. (2006) *J Lipid Res* **47**, 2028-2041

SUPPLEMENTAL FIGURE LEGENDS

SUPPL. FIG. 1. Histological analysis of seminiferous tubules from control (Kit^{W}) (*A*) and $Kit^{W\text{-}v}/Kit^{W}$ (*B*) testis. The seminiferous tubules of mutant mice testes (*B*) display conspicuous atrophy as compared to controls (*A*). The mutant seminiferous epithelium neither contains intact spermatocytes, nor round or elongating spermatids. Note, the mutant tubules show the phenotype of partial Sertoli cell-only syndrome with marked vacuolizations and numerous apoptotic germ cells. Semithin epon sections were stained with methylene blue–azure II. *White arrows*, Leydig cells; *yellow arrows*, Sertoli cell nuclei; *red arrows*, spermatogonia; *short orange arrows*, adluminal spermatocytes; *orange asterisks*, round spermatids; *red asterisks*, maturating spermatozoa; bar, 50 µm.

SUPPL. FIG. 2. Histological analysis of juvenile testes during postnatal development. During maturation of the seminiferous epithelium [*A*) P10, *B*) P14, *C*) P15 and *D*) P20, *E*) and *F*) P30] the remarkable increase in tubular size between P15 and P30 (*C-F*) is related to the formation of the adluminal compartment containing primarily pachytene primary spermatocytes and progressively spermatids (P20 – *D* and P30 – *F*). In parallel the number of Sertoli cell nuclei (*yellow* +: in this example 37 nuclei at P10 and 15 nuclei at P30) found in the cross section of a seminiferous tubule at P10 does not increase proportionally, but declines during maturation (P30) confirming published results (4). Semithin epon sections were stained with methylene blue–azure II. *White arrow*, Leydig cell; *yellow arrow*, Sertoli cell nucleus; *red arrow*, spermatogonia; *short orange arrow*, adluminal primary pachytene spermatocyte; *orange asterisk*, round spermatid; *red asterisk*, maturating spermatozoa; bar, *A*) - *E*) 50 µm, *F*) 10 µm.

SUPPL. FIG. 3. Histological and immunohistological localization of the blood-testis-barrier in seminiferous epithelium from a 18 day old C57BL/6 control testis. *A*) Methylene blue–azure II staining of semithin epon sections. Strands of tight junction complexes are clearly visible as dark blue lines (*black short arrows*), separating the basal compartment with speratogonia from the adluminal compartment displaying the columns of pachytene primary spermatocytes and round spermatids. *B*) Triple immunofluorescence for ZO-1 (*green*), claudin-11 (*red*) and nuclei (DAPI, *blue*) in a seminiferous tubule. ZO-1 and claudin 11 are components of the tight junction complexes. W*hite arrows*, Leydig cells; *yellow arrows,* Sertoli cell nuclei; *red arrows*, spermatogonia; *short orange arrows*, adluminal primary pachytene spermatocytes; *orange asterisks*, round spermatids; bar, *A* and *B*, 10 µm.

SUPPL. FIG. 4. HPLC-quantification of testicular GSLs from juvenile and pubertal testes at different stages of testicular development. GSLs were derivatized and separated by HPLC. Note, as neutral fucosylated GSLs appear (Fig. 2F) neutral GSLs increase remarkably between P15 and P25. Gangliosides (acidic GSLs) decrease significantly between P5 and P20, mainly due to changing levels of GM3 and GD3. GlcCer levels are not included by this method.

SUPPL. FIG. 5. Mass spectrometric analysis of gangliosides during postnatal testicular maturation. NanoESI-MS/MS characterization of complex neutral GSLs (*precursor ion scan m/z +204*) and gangliosides (*precursor ion scan m/z -87*) from control C57BL/6 testis. Signals for fucosylated VLC-PUFA GSLs (FucGA1, Gal(Fuc)GA1, GalNAc(Fuc)GA1 and GalNAcGal(Fuc)GA1 dominate at P20 with signals of Forssman lipid not exceeding 12 % of relative intensity. At P15, small signals (not more than 18 % of relative intensity) for fucosylated VLC-PUFA GSLs are found with dominant signals of Forssman lipid. At P10 no significant signals for VLC-PUFA GSLs are detectable. Signals of Forsmann lipid are dominant next to signals for Gb_4Cer. Signals for fucosylated VLC-PUFA gangliosides [Gal(Fuc)GM1, GalNAc(Fuc)GM1, GalNAcGal(Fuc)GM1] are not present at P10 and P15 but are detectable at P20, whereas signals for FucGM1(d18:1,16:0) are also detectable at P10 and P15. $GD3^{2-}$ signals are more intense than signals for $GT1^{3-}$ at P10 but decline at P15 and P20. Signals for GD3, GD1 and GT1 and GM3 correlate to compounds containing NeuNAc and NeuNGc and saturated or monounsaturated fatty acyl moieties with a chain length of 16 to 24 carbon atoms.

SUPPL. FIG. 6. Total juvenile testicular fatty acid compositions. *A*) Non-hydroxy fatty acid compositions *B*) α-Hydroxy fatty acid compositions. Signal intensities are plotted in percent of signal intensity measured for (α-hydroxy)palmitic acid from the corresponding age. Error bars represent standard deviation with n = 3. Non-hydroxy fatty acids were detected with nanoESI-mass spectrometry *MS1 scan*, α-hydroxy fatty acids with *neutral loss m +46 scan*. Note: Non-hydroxy and α-hydroxy VLC-PUFAs expression increases strongly from P15 to P25. Nevertheless, the non-hydroxy VLC-PUFA octacosapentaenic acid (28:5) is detected in minor amounts already at P6.

SUPPL. FIG. 7. Mass spectrometric analysis of phosphoglycerolipids and cholesteryl esters in comparison to sphingomyelins and ceramides during postnatal testicular maturation. NanoESI-MS/MS spectra of testicular lipids from 6 and 25 day old mice shown are a representative out of 3 different tissue pools for each age: phosphatidylcholine and sphingomyelin (*precursor ion scan m/z +184*), phosphatidylethanolamine (*neutral loss scan m +141*), and phosphatidylserine (*neutral loss scan m +185*), ceramide (*precursor ion scan m/z +264*), and cholesteryl esters (*precursor ion scan m/z +369*). Phosphatidylcholine, -ethanolamine, -serine, and cholesterylesters were detected from lipid extracts before and ceramide and sphingomyelin from lipid extracts after mild alkaline treatment. Note: testicular sphingomyelins and especially ceramides of 25 day old mice contain in contrast to phosphoglycerolipids (PC, PE, PS) and cholesteryl esters a significant amount of VLC-PUFA species. VLC-PUFAs may be incorporated into phosphatidylserines to a minor degree already at day 6.

SUPPL. FIG. 8. Testicular mRNA levels during juvenile postnatal development of enzymes involved in fatty acid elongation and desaturation as well as complex glycosphingolipid synthesis . Quantitative Real Time PCR of mRNAs from juvenile testes (P5 – P25). The mRNA was isolated from prepubertal testes at different points of development, transcribed into cDNA and subjected to qRT-PCR. *A*) ΔCT values [CT(*Cers*)-CT(*GAPDH*)] obtained from qRT-PCR were normalized to ΔCT of *Cers5*-mRNA (ΔΔCT) at P5 (see Fig. 4). Note: Whereas no changes were observed for *Siat9*-mRNA there is an increase of *Fut1*-, *Fut2*-, and *Galgt1*-mRNA until P25. Furthermore, *D6d*, *Elovl2*- and *Elovl5*-mRNA increase significantly from P10 to P25.

SUPPLEMENTAL TABLES

SUPPLEMENTAL TABLE 1: Primers used for qRT-PCR

Gene	Primer	Primer Sequence	Product size (bp)
Fut1	forward	5'– TTCCTGTCCTGAGCAGTCCT – 3'	150
	reverse	5' – GCATGCATCTCAGGTTGGAT – 3'	
Fut2	forward	5' – TACACAGCGACACAGCCAGA – 3'	109
	reverse	5' – TATCCCGTGAAACGCACATA – 3'	
Galgt1 / B4galnt1	forward	5' – GTTGGCTTCCCAAGTTGTGT – 3'	132
	reverse	5' – TCCATCCAGGAAGAATTCCA – 3'	
Siat9 / St3gal5	forward	5' – CAAGTGGCTTCAAGCAATGGT – 3'	120
	reverse	5' – GGGTTCAAAATCCTGAAGTGC – 3'	
D5d / Fads1 *	forward	5' – TGTGTGGGTGACACAGATGA – 3'	115
	reverse	5' – GTTGAAGGCTGATTGGTGAA – 3'	
D6d / Fads2 *	forward	5' – CCACCGACATTTCCAACAC – 3'	133
	reverse	5' – GGGCAGGTATTTCAGCTTCTT – 3'	
D9d / Scd1 *	forward	5' – TCAACTTCACCACGTTCTTCA – 3'	115
	reverse	5' – CTCCCGTCTCCAGTTCTCTT – 3'	
Elovl1	forward	5' – GGTGGGGGATAAAAATTGCT – 3'	106
	reverse	5' – CCAAGGGCAGACAATCCATA – 3'	
Elovl2	forward	5' – GACGCTGGTCATCCTGTTCT – 3'	105
	reverse	5' – GCTTTGGGGAAACCATTCTT – 3'	
Elovl3	forward	5' – TTTGCCATCTACACGGATGA – 3'	84
	reverse	5' – CGTGTCTCCCAGTTCAACAA – 3'	
Elovl4	forward	5' – GGGATCATACAACGCAGGAT – 3'	118
	reverse	5' – CTCAACGCCTTTCGATACAA – 3'	
Elovl5	forward	5' – CTCTCGGGTGGCTGTTCTT – 3'	98
	reverse	5' – AGAGGCCCCTTTCTTGTTGT – 3'	
Elovl6 *	forward	5' – ACAATGGACCTGTCAGCAAA– 3'	119
	reverse	5' –GTACCAGTGCAGGAAGATCAGT– 3'	
Elovl7	forward	5' – ATCGAGGACTGTGCGTTTTT – 3'	81
	reverse	5' – GGCGAGGACATGAGGAGATA – 3'	

*: For these mRNAs the primer sequences were taken from Wang et al. (5).

SUPPLEMENTAL FIGURES

Suppl. Fig. 1

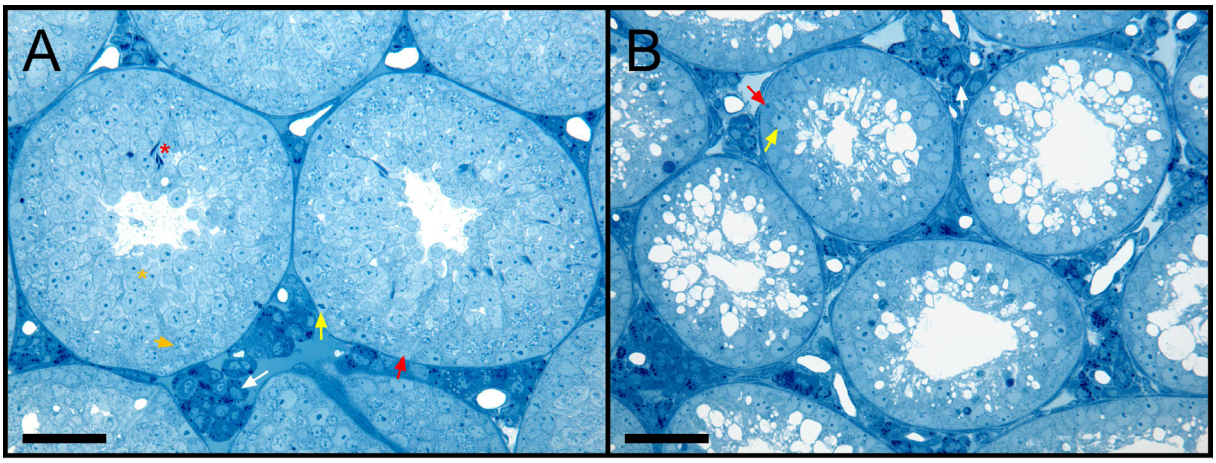

Suppl. Fig. 2

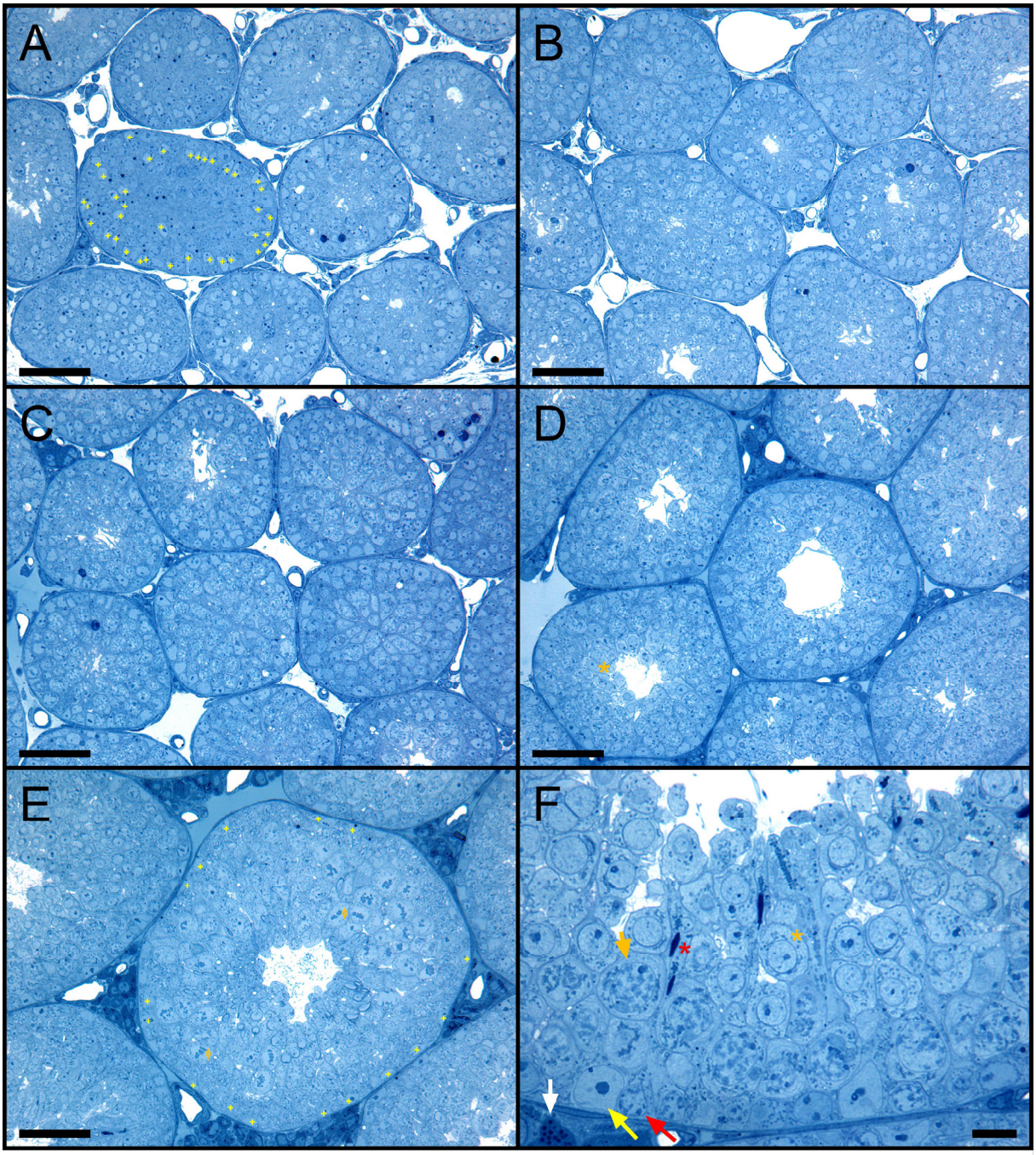

Suppl. Fig. 3

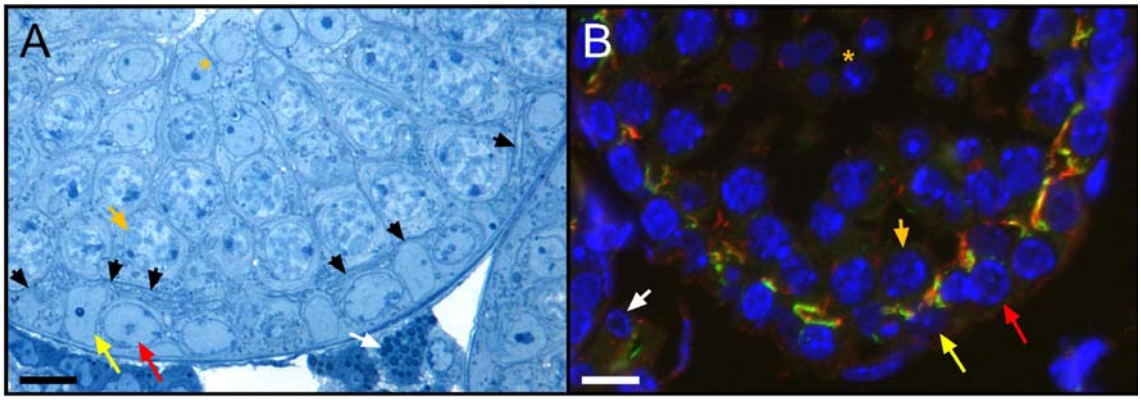

Suppl. Fig. 4

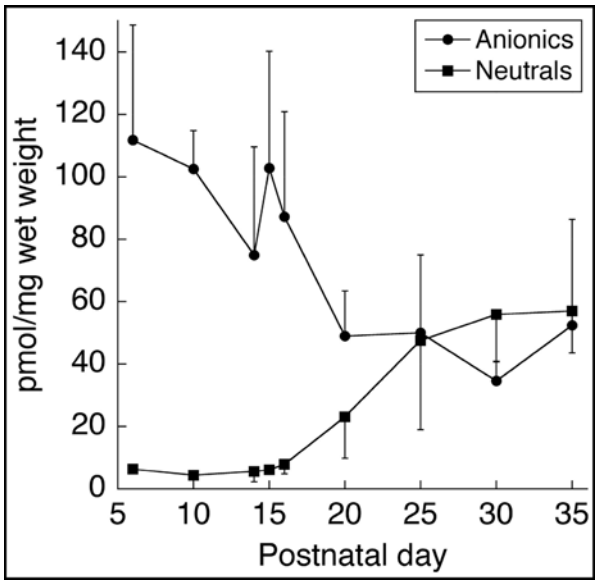

Suppl. Fig. 5

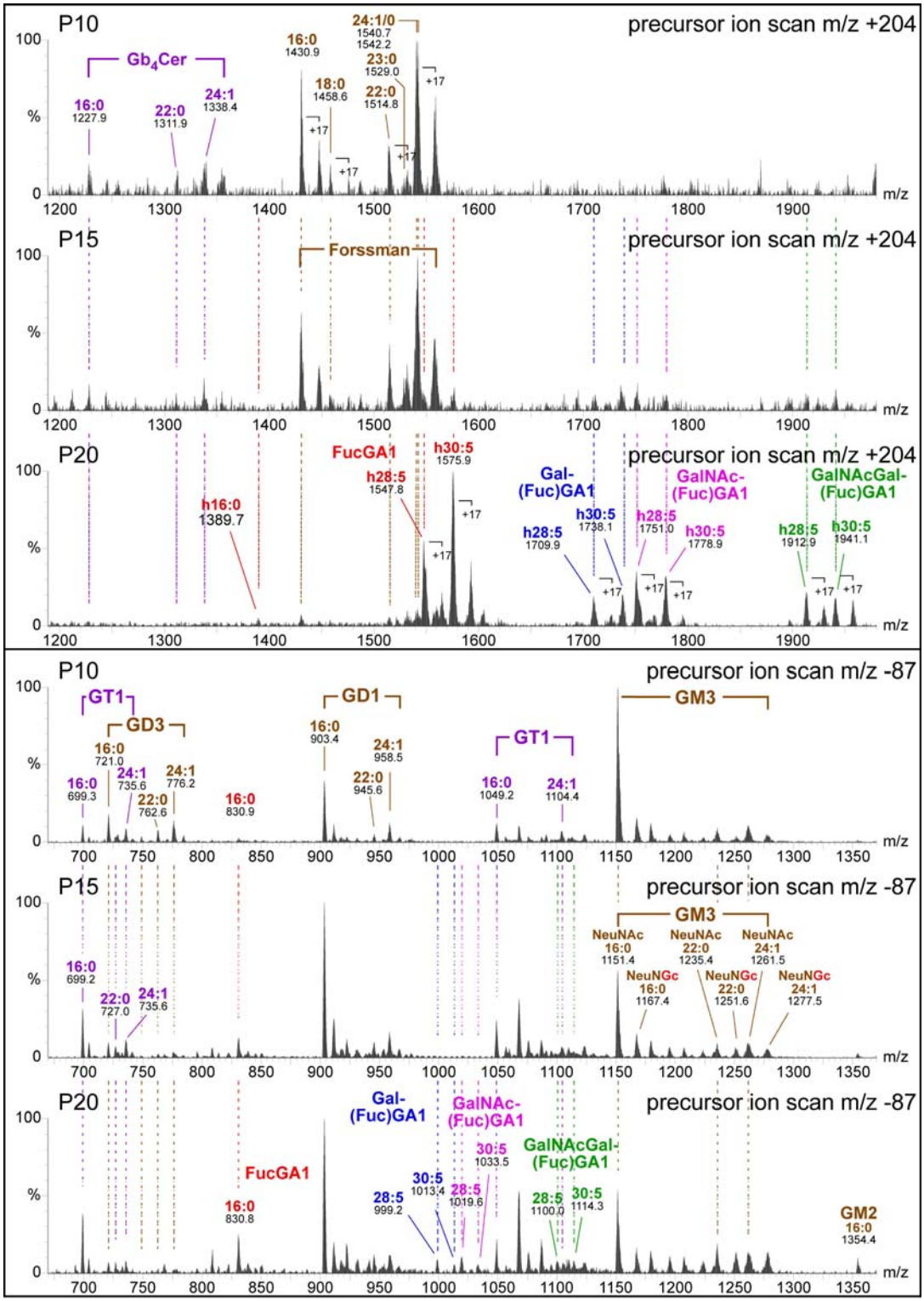
P10
precursor ion scan m/z +204
Gb4Cer
16:0 1227.9
22:0 1311.9
24:1 1338.4
16:0 1430.9
18:0 1458.6
24:1/0 1540.7 1542.2
23:0 1529.0
22:0 1514.8
P15
precursor ion scan m/z +204
Forssman
P20
precursor ion scan m/z +204
FucGA1
h30:5 1575.9
h28:5 1547.8
h16:0 1389.7
Gal-(Fuc)GA1
h28:5 1709.9
h30:5 1738.1
GalNAc-(Fuc)GA1
h28:5 1751.0
h30:5 1778.9
GalNAcGal-(Fuc)GA1
h28:5 1912.9
h30:5 1941.1
P10
precursor ion scan m/z -87
GT1
GD3
16:0 721.0
16:0 699.3
24:1 735.6
24:1 776.2
22:0 762.6
16:0 830.9
GD1
16:0 903.4
24:1 958.5
22:0 945.6
GT1
16:0 1049.2
24:1 1104.4
GM3
P15
precursor ion scan m/z -87
GM3
NeuNAc 16:0 1151.4
NeuNAc 22:0 1235.4
NeuNAc 24:1 1261.5
NeuNGc 16:0 1167.4
NeuNGc 22:0 1251.6
NeuNGc 24:1 1277.5
16:0 699.2
22:0 727.0
24:1 735.6
P20
precursor ion scan m/z -87
Gal-(Fuc)GA1
GalNAc-(Fuc)GA1
GalNAcGal-(Fuc)GA1
FucGA1
16:0 830.8
28:5 999.2
30:5 1013.4
28:5 1019.6
30:5 1033.5
28:5 1100.0
30:5 1114.3
GM2 16:0 1354.4
m/z
%

Suppl. Fig. 6

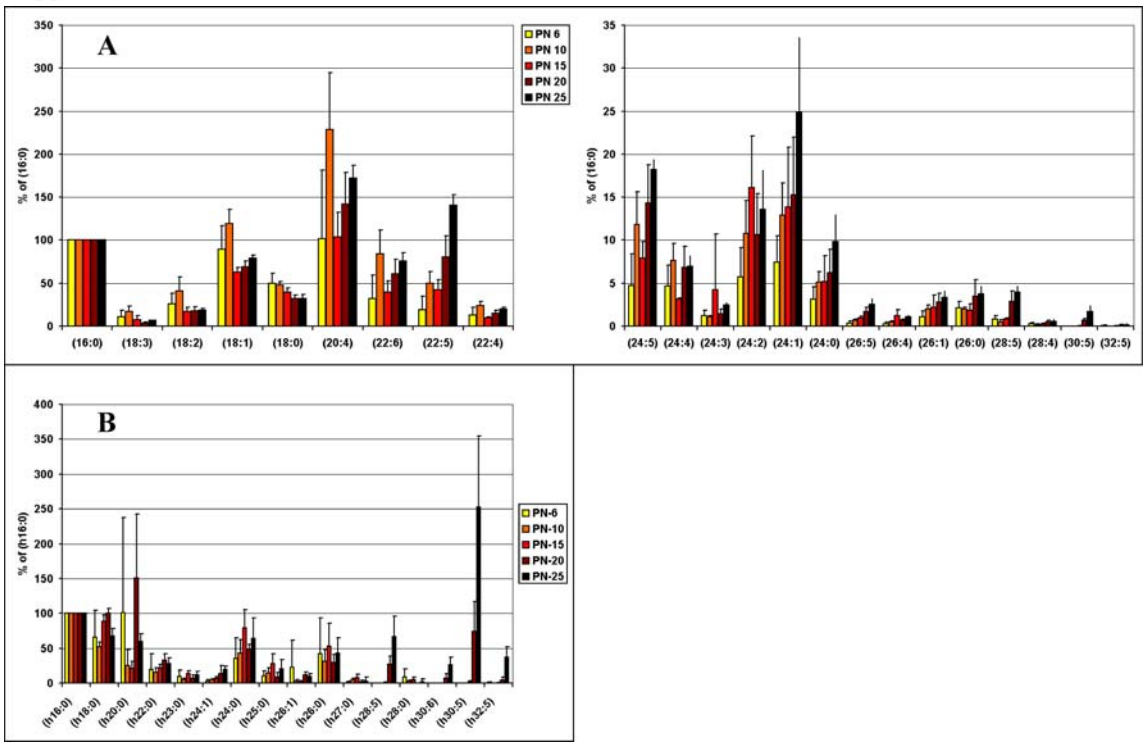
A
PN 6
PN 10
PN 15
PN 20
PN 25
% of (16:0)
(16:0) (18:3) (18:2) (18:1) (18:0) (20:4) (22:6) (22:5) (22:4)
(24:5) (24:4) (24:3) (24:2) (24:1) (24:0) (26:5) (26:4) (26:1) (26:0) (28:5) (28:4) (30:5) (32:5)
B
PN-6
PN-10
PN-15
PN-20
PN-25
% of (h16:0)
(h16:0) (h18:0) (h20:0) (h22:0) (h23:0) (h24:1) (h24:0) (h25:0) (h26:1) (h26:0) (h27:0) (h28:5) (h28:0) (h30:6) (h30:5) (h32:5)

Suppl. Fig. 7

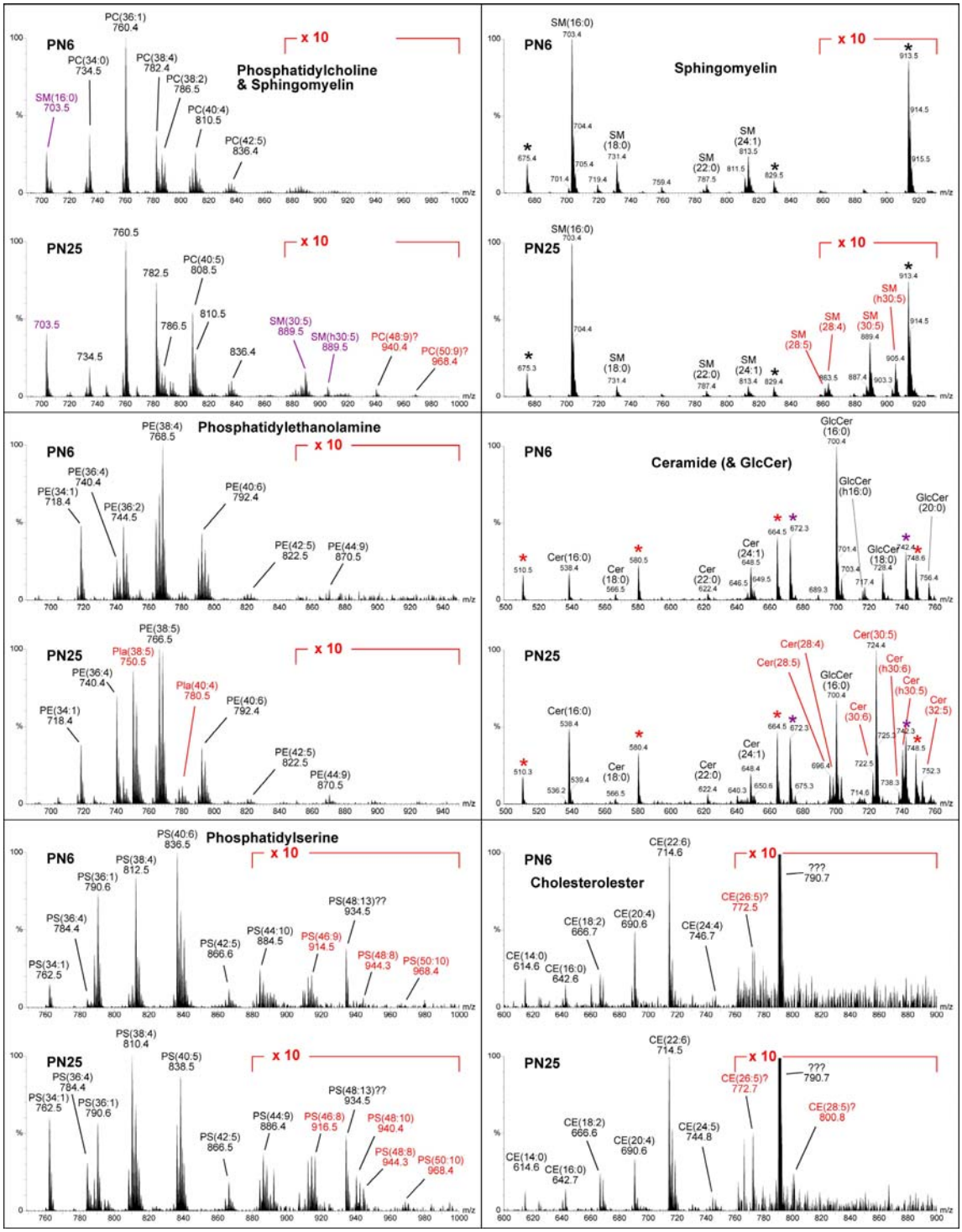
PN6
Phosphatidylcholine & Sphingomyelin
PC(36:1) 760.4
PC(34:0) 734.5
PC(38:4) 782.4
PC(38:2) 786.5
PC(40:4) 810.5
PC(42:5) 836.4
SM(16:0) 703.5
x 10
PN25
760.5
782.5
PC(40:5) 808.5
810.5
786.5
703.5
734.5
836.4
SM(30:5) 889.5
SM(h30:5) 889.5
PC(48:9)? 940.4
PC(50:9)? 958.4
Sphingomyelin
SM(16:0) 703.4
SM (18:0) 731.4
SM (22:0) 787.5
SM (24:1) 813.5
SM (28:4)
SM (28:5)
SM (30:5) 889.4
SM (h30:5) 914.5
Phosphatidylethanolamine
PE(38:4) 768.5
PE(36:4) 740.4
PE(34:1) 718.4
PE(36:2) 744.5
PE(40:6) 792.4
PE(42:5) 822.5
PE(44:9) 870.5
PE(38:5) 766.5
Pla(38:5) 750.5
Pla(40:4) 780.5
Ceramide (& GlcCer)
GlcCer (16:0) 700.4
GlcCer (h16:0)
GlcCer (20:0)
Cer(16:0) 538.4
Cer (18:0) 566.5
Cer (22:0) 622.4
Cer (24:1) 648.5
GlcCer (18:0) 728.4
Cer(28:4)
Cer(28:5)
Cer(30:5) 724.4
Cer (h30:6)
Cer (h30:5)
Cer (30:6)
Cer (32:5)
Phosphatidylserine
PS(40:6) 836.5
PS(38:4) 812.5
PS(36:1) 790.6
PS(36:4) 784.4
PS(34:1) 762.5
PS(42:5) 866.6
PS(44:10) 884.5
PS(46:9) 914.5
PS(48:13)?? 934.5
PS(48:8) 944.3
PS(50:10) 968.4
PS(38:4) 810.4
PS(40:5) 838.5
PS(44:9) 886.4
PS(46:8) 916.5
PS(48:10) 940.4
Cholesterolester
CE(22:6) 714.6
??? 790.7
CE(26:5)? 772.5
CE(18:2) 666.7
CE(20:4) 690.6
CE(24:4) 746.7
CE(14:0) 614.6
CE(16:0) 642.6
CE(24:5) 744.8
CE(28:5)? 800.8

Suppl. Fig. 8

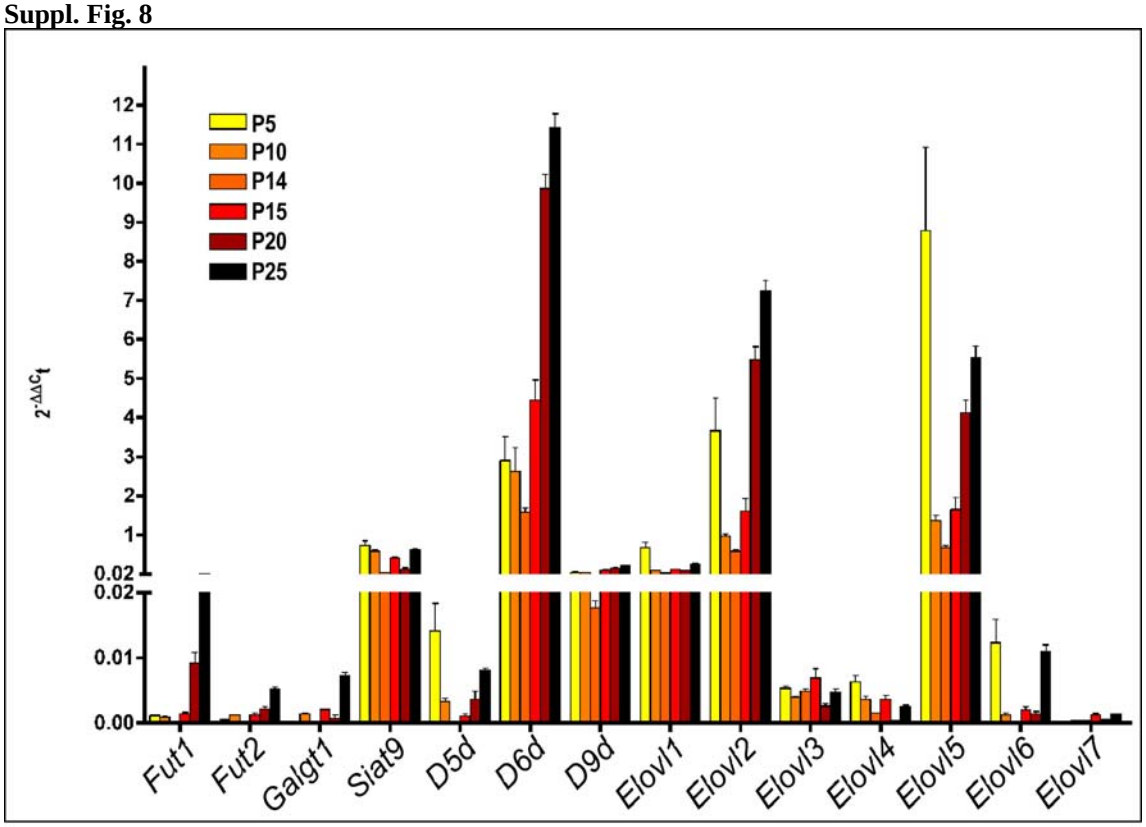
P5
P10
P14
P15
P20
P25
$2^{-\Delta\Delta C_t}$
12
11
10
9
8
7
6
5
4
3
2
1
0.02
0.02
0.01
0.00
Fut1
Fut2
Galgt1
Siat9
D5d
D6d
D9d
Elovl1
Elovl2
Elovl3
Elovl4
Elovl5
Elovl6
Elovl7